Letter submitted to *Physics of Fluids*

Enhanced upswing in immersed collisions of tethered spheres

Hui-Chi Hsu and Hervé Capart

Department of Civil Engineering and Hydrotech Research Institute, National Taiwan University, No.1, Sec.4, Roosevelt Road, Taipei 10617, Taiwan.

Experiments and simplified computations are performed to study the influence of liquid motions on the dynamics of immersed pendulums. The pendulums consist of tethered spheres, swinging alone or colliding with one another in liquid initially at rest. Surprisingly, oscillations initiated in identical fashion are found to be damped less rapidly when spheres collide. Using refractive-index-matched materials and laser-illuminated tracers to visualize the liquid flow between and around the spheres, we link this effect to the response of wake vortices. Set in motion by impact, a sphere emerges virtually wake-free from the collision, leading to reduced drag and enhanced upswing.

Like dry granular flows,[1,2] liquid-granular flows are strongly affected by frequent collisions between solid particles.[3,4] To account for these collisional effects, researchers have sought to extend kinetic theories and discrete particle simulations developed first for dry granular media to flows of liquid-granular mixtures.[5,6] Coupling between solid and liquid motions, however, makes it more difficult to ascertain the influence of immersed collisions on the stress and energy balance of mixture flows. Assuming an ideal fluid, liquid inertia influences colliding particles by contributing to their apparent momentum and by mediating interaction forces.[7,8] For real fluids, recent studies of immersed particle-wall[9,10] and particle-particle collisions[11] have shown how particle rebound is damped by liquid viscosity. The liquid vorticity may also

play an active role, responding to impact and influencing the striking body in particle-wall collisions.[12,13] For particle-particle collisions, the role played by vortex motions has not yet been examined. In this Letter, we show that vortex responses to immersed particle-particle collisions can exert a significant and surprising influence on the particle dynamics. In immersed pendulum experiments conducted at high Reynolds and Stokes numbers, we find that the oscillations of spherical bobs are damped less rapidly when they collide with one another than when they swing alone. Our findings suggest that wake responses to particle contacts are important in liquid-granular flows, which in turn intervene in a variety of geophysical and industrial processes.

Experiments with tethered spheres have been used to study fluid resistance[14] and dry collisions,[15] and more recently to investigate sphere-vortex interactions[16] and immersed collisions.[9,11] To clarify the interplay between vortex motions and immersed collisions, we conducted experiments with both isolated and colliding spheres, in the pendulum configurations illustrated in Fig. 1. Each pendulum has height H = 180 mm and features a spherical bob of diameter D = 40 mm, tethered to rigid supports and immersed in a liquid pool in a tank of internal dimensions 500 × 400 × 350 mm^3. To provide some lateral restraint, a bifilar suspension is adopted. Oblique strings (0.3 mm in diameter) are attached to small screws mounted on opposite sides of each sphere, and suspended from rigid supports on both sides of the plane of swing. Sphere motion is initiated by gentle manual release from a rigid railed guide, with the released pendulum starting from angle $\theta_0 = -1$ rad. In the single pendulum experiments (Fig. 1a), the released sphere oscillates alone in the liquid. In the colliding pendulums experiments (Fig. 1b), by contrast, the released sphere impacts the bob of another identical pendulum, initially at rest and suspended one sphere diameter away.

To facilitate observation, the refractive-index-matched transparent materials proposed in ref. 17 are used. The solid spheres are made of polymethyl methacrylate (PMMA, density ρ_S = 1,190 kg m^{-3}) and bathed in the liquid para-cymene (benzene, 1-methyl-4-(1-methylethyl)-; density ρ_L = 860 kg m^{-3}, viscosity μ_L =1.02 × 10^{-3} Pa s). The materials share the same index of refraction n = 1.49, allowing unhindered light passage and visual access through the spheres. We exploit this transparency to obtain stereoscopic measurements of the bob motions, and to visualize liquid motions between and around the bobs using laser-illuminated tracers. A binocular camera arrangement is used to obtain stereoscopic measurements of the sphere motions, based on the methods documented in ref. 18. The centroids of the screw heads mounted on both sides of each sphere are extracted from synchronized images (resolution 778 by 1032 pixels) acquired at frame rate 20 Hz (AVT Marlin F-080B cameras operated with open-source software Coriander). Their three-dimensional positions are then determined by ray intersection based on calibrated projective transforms followed by a distortion correction, yielding a spatial accuracy of 0.6 mm. Sphere centres are obtained as the midpoints between the left and right screw heads, yielding an accuracy of 3.5 mrad on the angles of swing. Transverse excursions left and right of the plane of swing due to lateral sway do not exceed 4 mm. To process the angle histories, different experiments are first given a common time origin by finding the instant at which the released bob crosses angle $\theta = -0.2$ rad during its first downswing. Angular velocities are obtained by differencing, and extrapolated to the times of collision to obtain pre- and post-collision velocities. To keep collisions sharp, angle histories for the colliding bobs are split into segments at successive impacts, then merged into inner and outer modes before averaging multiple tests.

Measured swing histories for the single and colliding pendulums are compared in Fig. 2a. The data are extracted from 80 stereoscopic experiments, conducted in alternating series of 10

single pendulum and 10 collision tests, save for 5 out-of-sequence runs added to replace 5 runs in which camera synchronization failed. As could be expected, the immersed bobs undergo subcritically damped oscillations. For colliding pendulums, these oscillations are interrupted by repeated impacts. The released bob swings down, comes to an abrupt near-stop at the first collision as the target bob swings up, before the bobs collide again upon reverse downswing, and so on. During the first downswing, the released bobs in the single and colliding pendulums experiments exhibit indistinguishable angle histories, attaining maximum angular velocities $\dot{\theta}^{\max} = 2.221 \pm 0.024$ rad s^{-1} and $\dot{\theta}_1^{\max} = 2.215 \pm 0.025$ rad s^{-1} respectively (uncertainties are one standard deviation for repeated experiments). After the first collision, however, the curves of the single and target bobs diverge. Surprisingly, the bob set in motion by impact rises higher than the isolated bob, attaining a maximum upswing angle $\theta_2^{\max} = 0.333 \pm 0.017$ rad, compared to value $\theta^{\max} = 0.271 \pm 0.021$ rad for the single bob (Fig. 3). Moreover, this enhanced upswing is sustained over at least one more cycle interrupted by two further collisions (Fig. 2a).

The result is surprising because, for colliding pendulums, kinetic energy is partially shared by the two bobs and partly lost due to the collisions. At each impact, the bobs exchange their angular velocities, with some loss that can be described by Newton's coefficient of restitution

$$e = -(\dot{\theta}_2' - \dot{\theta}_1')/(\dot{\theta}_2 - \dot{\theta}_1), \qquad (1)$$

where $\dot{\theta}_{1,2}$ and $\dot{\theta}_{1,2}'$ are the angular velocities immediately before and after collision. Values e estimated from the measured angle histories (Fig. 4) trend downwards with successive collisions, decreasing from $e = 0.97 \pm 0.04$ at the first collision to $e = 0.84 \pm 0.03$ at the eighth impact (uncertainties are one standard deviation). This agrees with previous immersed collision experiments,[9–11] which indicate that the restitution coefficient decreases

with lower impact speed, as measured by Stokes number $St = \frac{2}{9}\rho_S DH\,|\dot{\theta}_2 - \dot{\theta}_1|\cos\theta_1 / \mu_L$.[19] The enhanced upswing observed despite these collisional losses indicates that they are overshadowed by other effects, which we characterize using the following simple mathematical model. For the single pendulum, an equation of motion can be written

$$(\rho_S + \rho_L a)\ddot{\theta} = -(\rho_S - \rho_L)\frac{g}{H}\sin\theta - \tfrac{3}{4}\rho_L \frac{H}{D} c\,|\dot{\theta}|\,\dot{\theta}, \qquad (2)$$

where $\ddot{\theta}$ is the angular acceleration, $a = \frac{1}{2}$ is the added mass coefficient for an isolated immersed sphere, g is the gravitational constant, and c is a phenomenological drag coefficient influenced by the Reynolds number and particle acceleration.[20,21] For two interacting pendulums, likewise, coupled equations of motion can be written

$$(\rho_S \mathbf{I} + \rho_L \mathbf{A})\begin{bmatrix}\ddot{\theta}_1 \\ \ddot{\theta}_2\end{bmatrix} = -(\rho_S - \rho_L)\frac{g}{H}\begin{bmatrix}\sin\theta_1 \\ \sin\theta_2\end{bmatrix} + \rho_L \mathbf{B}\begin{bmatrix}\dot{\theta}_1^2 \\ \dot{\theta}_1\dot{\theta}_2 \\ \dot{\theta}_2^2\end{bmatrix} - \tfrac{3}{4}\rho_L \frac{H}{D}\begin{bmatrix}c_1\,|\dot{\theta}_1|\,\dot{\theta}_1 \\ c_2\,|\dot{\theta}_2|\,\dot{\theta}_2\end{bmatrix}, \qquad (3)$$

where $\mathbf{I}$ is the identity matrix, and where added mass matrix $\mathbf{A}$ and Bernoulli matrix $\mathbf{B}$ describe pressure forces associated with the irrotational liquid flow induced by the sphere motions. These terms can be derived by a Lagrangian approach[22] or by the Bernoulli theorem.[23] The resulting coefficients A_{ij} and B_{ij} are dimensionless functions of angles θ_1, θ_2 and aspect ratio H/D which do not depend on the angular velocities and accelerations. In the last term of eq. 3, parameters c_1 and c_2 are again phenomenological drag coefficients. They are needed to account for the real fluid effects left out by the other terms. To capture pendulum impacts, eq. 3 is supplemented by the collision rules

$$\dot{\theta}_1' = \tfrac{1}{2}(\dot{\theta}_1 + \dot{\theta}_2) + \tfrac{1}{2}e(\dot{\theta}_2 - \dot{\theta}_1), \qquad \dot{\theta}_2' = \tfrac{1}{2}(\dot{\theta}_1 + \dot{\theta}_2) - \tfrac{1}{2}e(\dot{\theta}_2 - \dot{\theta}_1), \qquad (4)$$

where we substitute the measured values of e at successive collisions. Irrotational flow is computed by solving the Laplace equation using the method of fundamental solutions.[24,25] The resulting pressure forces are integrated using 400 collocation nodes along the surface of

each sphere. Simulated angle histories $\theta(t)$, $\theta_1(t)$ and $\theta_2(t)$ are then obtained by integrating eq. 2 or 3 in time using the Euler-Cromer scheme (with time step $\Delta t = 1$ ms), save for discrete collision events where eq. 4 is applied.[26]

Zero-drag solutions of eqs 2-4 obtained by setting $c = c_1 = c_2 = 0$ can reproduce various features of the observed angle histories. First, the periods of swing are close to the theoretical value $T = 2\pi\sqrt{(\rho_S + \frac{1}{2}\rho_L)/(\rho_S - \rho_L)}\sqrt{H/g}$ for small oscillations of an isolated sphere in an ideal fluid.[14] Drag-free computations also capture the small pre-collision motion of the target bob observed in Fig. 2a, and documented earlier in ref. 11. It is due to a short-range repulsive force described by the Bernoulli term in eq. 3, associated with a transient pressure rise between the spheres before and after collision. Over repeated collisions, this interaction leads to entrainment coupling between the two bobs, which also gradually synchronize their motions due to the partially inelastic rebound ($e < 1$). None of these effects, however, accounts for the difference in upswing observed between the single pendulum and colliding pendulums experiments. For this purpose, it is necessary to tune drag coefficients c, c_1 and c_2, resulting in the simulated angle histories shown in Fig. 2b. For the single pendulum case, we find that a good fit is obtained by setting $c = = 0.95$ for the first arc, then decreasing this value by half after the first reversal of direction at the apogee $\theta = \theta_{max}$. For the colliding pendulums, we set $c_1 = c_2 = C$ for simplicity, but allow C to change over time. A value $C = 0.95$ identical to the single pendulum case is adopted for the downswing, but must be reduced by a factor of three at the first collision to reproduce the observed upswing and ensuing oscillations. Thus a reduction in drag is detected in both cases, but the reduction is stronger (threefold instead of twofold) and occurs earlier (first perigee instead of first apogee) for the colliding pendulums.

To elucidate this contrast in behavior, we examine the corresponding flow patterns. Liquid motions in the plane of symmetry are made visible by seeding the liquid with micro-particles (50 μm in diameter, density 1,020 kg m^{-3}), and illuminating the plane using a laser light sheet (Argon Ion Laser operating at a power of approximately 2 W). A monochrome camera (IDT X-stream vision) records the flow from the side at a frame rate of 100 Hz and a resolution of approximately 5 pixel mm^{-1}. Thanks to refractive index matching, shadows and caustics are avoided, and tracers are illuminated evenly around and between the spheres. Velocity vectors are identified semi-manually based on four successive frames merged into a colour image using a blue-red-green-blue coding scheme. Vectors are then transferred to a regular grid using natural neighbor interpolation.

Measured flow fields obtained in this fashion are presented in Figs 5 and 6, depicting respectively a single pendulum and two colliding pendulums. As the single pendulum reaches its first perigee (Fig. 5b), the spherical bob slows down and gets overtaken from below by its own wake. The strong rotational wake induces a fore-aft pressure difference around the sphere, which is the main source of drag at these high Reynolds numbers (up to 10^4 during the first downswing). As the bob reaches its apogee (Fig. 5d), the pendulum acts like a sling and releases a traveling vortex ring that propagates obliquely downwards. Flow fields for the colliding pendulums are presented in Fig. 6. Panels 6a and 6b show the flow immediately before and after the first collision. As the striking bob transmits its impulse to the initially static bob, the rotational and irrotational components of the flow respond differently to the collision. Tied to the solid body motions, the irrotational component (associated with added mass) is transferred from one bob to another. The rotational component, however, is not affected and persists in the wake of the arrested bob (Fig. 6b).[27] After the collision (Fig. 6c), the vortex wake of the arrested bob splits into a downwards vortex ring below and a patch of

counter-clockwise secondary vorticity above. Most importantly, the upswinging bob escapes from the collision nearly wake-free, with a surrounding liquid flow that closely approximates the symmetric template of irrotational theory. Because the pressure distribution likewise more nearly satisfies fore-aft symmetry, reduced drag on the upswinging bob is expected. Weak patches of wake vorticity are revealed when the bob reaches its apogee (Fig. 6d), but these are nowhere near as strong as the original wake of the downswinging bob.

The above interpretation can be substantiated further by examining the liquid pathlines associated with the full downswing-collision-upswing sequence. Fig. 7a shows a long exposure image obtained from a sequence of frames by recording at each pixel the brightest illumination encountered during the sequence. The resulting image records laser-illuminated tracer motions as well as successive bob outlines, with especially bright halos recorded when spheres are at rest. This makes the spheres appear to interpenetrate at the centre of the image, because the impacting sphere comes to rest slightly to the right of its equilibrium position. For comparison, Fig. 7b shows simulated pathlines, computed under the assumption of irrotational flow around spheres moving according to the simulated angle histories of Fig. 2b. As could be expected, these irrotational pathlines cannot reproduce the flow pattern in the wake of the released sphere, nor its ensuing transformation into a downwards jet associated with the vortex ring. They do, however, provide a fairly accurate portrait of the liquid motions near the impact and around the upswinging target bob. Liquid parcels are pushed out of the gap upon approach of the impacting bob, and then suddenly reverse direction at the collision to generate cusped pathlines. From collision to apogee, furthermore, the pathlines around the upswinging bob form looping elastica that are characteristic of irrotational flow around moving spheres.[28]

In summary, we have documented in this work the significant influence of vortex motions on the dynamics of immersed pendulums, whether they swing alone or collide with one another.

When pendulums collide, the target bob receives its impulse from the striking bob, but starts afresh without a vortical wake, leading to reduced drag and enhanced upswing. These results suggest that, at the high Stokes and Reynolds numbers considered in this study, wake responses are at least as important as inelastic restitution when evaluating the influence of immersed collisions on the pace of mechanical energy dissipation in solid-liquid mixtures.

This work was supported by the National Science Council, Taiwan. We thank Chin-Chou Chu and Hsien-Ter Chou for lending the laser and high-speed camera, Ching-Biao Liao for useful discussions, and Der-Liang Young for advising the method of fundamental solutions.

References and footnotes

[1] J. T. Jenkins and S. B. Savage, "A theory for the rapid flow of identical, smooth, nearly elastic, spherical particles," J. Fluid Mech. **130**, 187 (1983).

[2] I. Goldhirsch, "Rapid granular flows," Annu. Rev. Fluid Mech. **35**, 267 (2003).

[3] R. A. Bagnold, "Experiments on a gravity-free dispersion of large solid spheres in a Newtonian fluid under shear," Proc. Roy. Soc. London A **225**, 49 (1954).

[4] A. Armanini, H. Capart, L. Fraccarollo, and M. Larcher, "Rheological stratification in experimental free-surface flows of granular-liquid mixtures," J. Fluid Mech. **532**, 269 (2005).

[5] J. T. Jenkins and D. M. Hanes, "Collisional sheet-flow of sediment driven by a turbulent fluid," J. Fluid Mech. **370**, 29 (1998).

[6] T. G. Drake and J. Calantoni, "Discrete particle model for sheet-flow sediment transport in the nearshore," J. Geophys. Res. **106**, 19859 (2001).

[7] A. S. Sangani and A. K. Didwania, "Dynamic simulations of flows of bubbly liquids at large Reynolds numbers," J. Fluid Mech. **250**, 307 (1993).

[8] H. F. Bulthuis, A. Prosperetti, and A. S. Sangani, "Particle stress in disperse 2-phase potential flow," J. Fluid Mech. **294**, 1 (1995).

[9] G. G. Joseph, R. Zenit, M. L. Hunt, and A. M. Rosenwinkel, "Particle-wall collisions in a viscous fluid," J. Fluid Mech. **433**, 329 (2001).

[10] P. Gondret, M. Lance, and L. Petit, "Bouncing motion of spherical particles in fluids," Phys. Fluids **14**, 643 (2002).

[11] F.-L. Yang and M. L. Hunt, "Dynamics of particle-particle collisions in a viscous liquid," Phys. Fluids **18**, 121506 (2006).

[12] G. G. Joseph, "Collisional dynamics of macroscopic particles in a viscous fluid," PhD thesis, California Institute of Technology, Pasadena, California (2003).

[13] T. Leweke, M. C. Thompson, and K. Hourigan, "Vortex dynamics associated with the collision of a sphere with a wall," Phys. Fluids **16**, L74 (2004).

[14] G. G. Stokes, "On the effect of the internal friction of fluids on the motion of pendulums," Trans. Cambridge Phil. Soc. **9**, 8 (1851).

[15] F. Herrmann and M. Seitz, "How does the ball-chain work?" Am. J. Phys. **50**, 977 (1982).

[16] R. N. Govardhan and C. H. K. Williamson, "Vortex-induced vibrations of a sphere," J. Fluid Mech. **531**, 11 (2005).

[17] S. J. Haam, R. S. Brodkey, I. Fort, L. Klaboch, M. Placnik, and V. Vanecek, "Laser Doppler anemometry measurements in an index of refraction matched column in the presence of dispersed beads – Part I," Int. J. Multiphase Flow **26**, 1401 (2000).

[18] B. Spinewine, H. Capart, M. Larcher, and Y. Zech, "Three-dimensional Voronoï imaging methods for the measurement of near-wall particulate flows," Exp. Fluids **34**, 227 (2003).

[19] This behavior involves elastohydrodynamic effects, acting over the very short time (not resolved by our measurements) during which spheres come in close contact [see R. H. Davis,

J.-M. Serayssol, and E. J. Hinch, "The elastohydrodynamic collision of two spheres," J. Fluid Mech. **163**, 479 (1986)].

[20]S. K. Karanfilian and T. J. Kotas, "Drag on a sphere in unsteady motion in a liquid at rest," J. Fluid Mech. **87**, 85 (1978).

[21]A more refined analysis would model the unsteady drag associated with vortex shedding [see M. S. Howe, G. C. Lauchle, and J. Wang, "Aerodynamic lift and drag fluctuations of a sphere," J. Fluid Mech **436**, 41 (2001)] or resort to direct numerical simulation of the flow [see M. C. Thompson, K. Hourigan, A. Cheung, and T. Leweke, "Hydrodynamics of a particle impact on a wall," Appl. Math. Modelling **30**, 1356 (2006)].

[22]P. Smereka, "On the motion of bubbles in a periodic box," J. Fluid Mech. **254**, 79 (1993).

[23]J. Koiller, "Note on coupled motions of vortices and rigid bodies," Phys. Lett. A **120**, 391 (1987).

[24]A. Bogomolny, "Fundamental-solutions method for elliptic boundary-value problems," SIAM J. Numer. Anal. **22**, 644 (1985).

[25]C. C. Tsai, D. L. Young, D. C. Lo, and T. K. Wong, "Method of fundamental solutions for three-dimensional Stokes flow in exterior field," ASCE J. Eng. Mech. **132**, 317 (2006).

[26]Computational accuracy was checked by verifying conservation of mechanical energy to within 0.5 % for immersed bobs colliding under conditions of zero drag and elastic rebound.

[27]This illustrates Kelvin's view that vortex motions are those that persist when boundary motions cease [Lord Kelvin, "On vortex motion," Trans. Roy. Soc. Edinburgh **25**, 217 (1867)].

[28]C. Darwin, "Note on hydrodynamics," Proc. Camb. Phil. Soc. **49**, 342 (1953).

[29]Of the 320 collision events covered by the tests, 3 could not be analyzed due to missing data, and 15 outliers more than 3 inter-quartile distances away from the median were excluded from the statistics.

Figure legends

FIG. 1. Geometry of the immersed pendulum tests: (a) single pendulum, (b) colliding pendulums. Gray silhouettes show the equilibrium positions of the spherical bobs, dashed lines their starting positions, and solid lines their instantaneous positions.

FIG. 2. Angle histories for single and colliding pendulums: (a) measured curves, representing the mean of 40 experiments, with error bars showing the standard deviation; (b) computational simulations. In each panel, the thin solid line represents the angle history $\theta(t)$ of the single pendulum, whereas thick dashed and solid lines represent the angle histories $\theta_1(t)$ and $\theta_2(t)$ of the colliding pendulums.

FIG 3. Measured maximum upswing angle and downswing angular velocity. Data for a single pendulum are represented by hollow circles (white histogram), and for colliding pendulums by filled triangles (black histogram). Higher upswing is observed for colliding pendulums despite indistinguishable maximum angular velocities during downswing.

FIG. 4. Variation of the coefficient of restitution with the Stokes number for successive collisions. Our data (black squares) are compared with measurements by Gondret et al. (ref. 10, hollow circles) for immersed sphere-wall impacts, and by Yang and Hunt (ref. 11, hollow triangles) for immersed normal collisions between spheres. Each of our data point represents a mean value averaged from 40 tests, with error bars showing the standard deviations.[29]

FIG. 5. Measured flow fields at successive stages in the motion of a single pendulum: (a) downswing, (b) perigee, (c) upswing, and (d) apogee.

FIG. 6. Measured flow fields at successive stages in the motions of colliding pendulums: (a) perigee right before collision, (b) perigee right after collision, (c) upswing, and (d) apogee.

FIG. 7. Liquid pathlines around colliding pendulums, from release to first apogee: (a) experimental long exposure image of the laser-illuminated symmetry plane, (b) simulated pathlines of passive tracers randomly dispersed in the plane and undergoing irrotational flow around the moving spheres. The dashed outline denotes the initial position of the target sphere, and solid outlines denote the right-most positions of the bobs at angles $\theta_1^{\max}$ and $\theta_2^{\max}$.

Figures

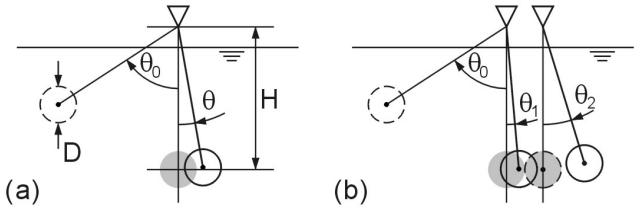

Figure 1

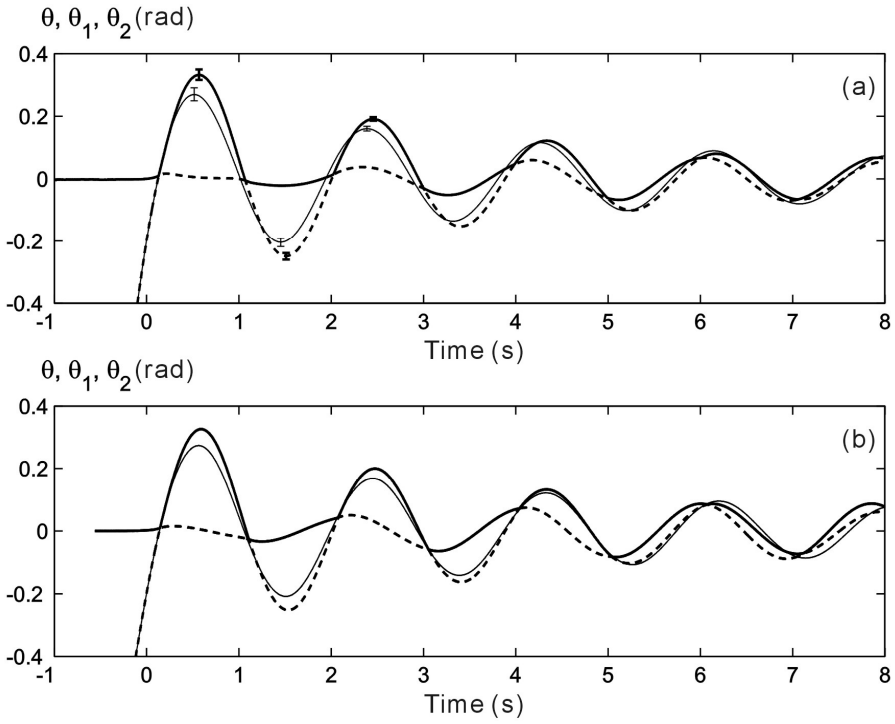

Figure 2

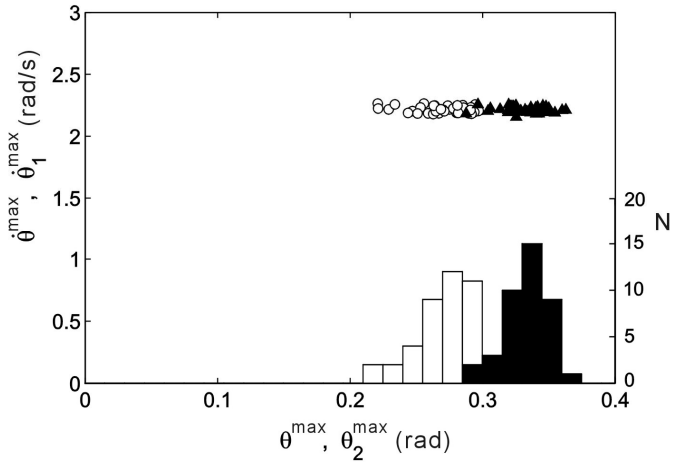

Figure 3

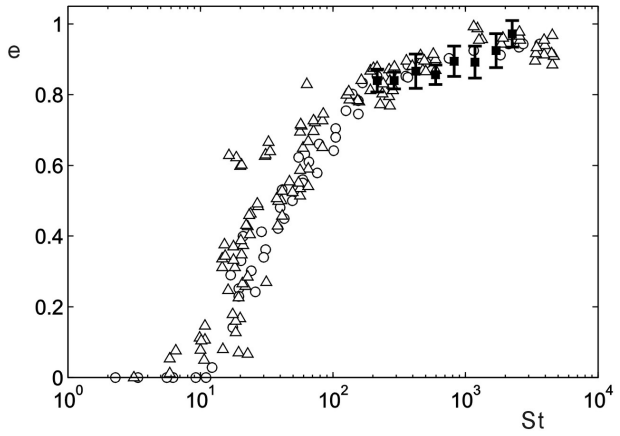

Figure 4

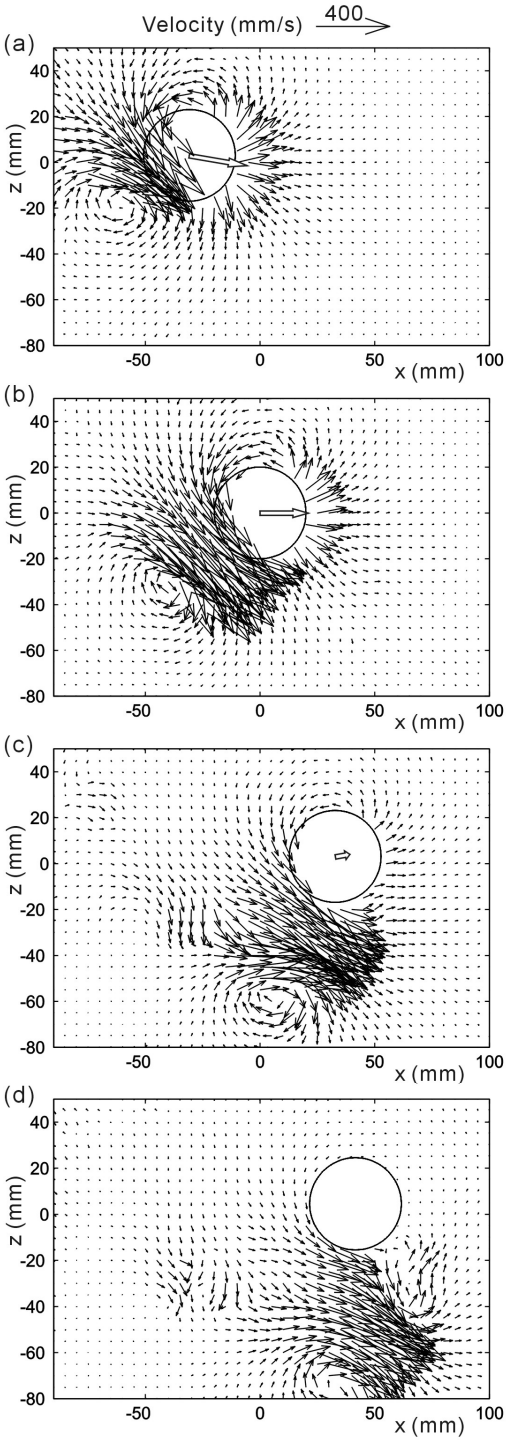

Figure 5

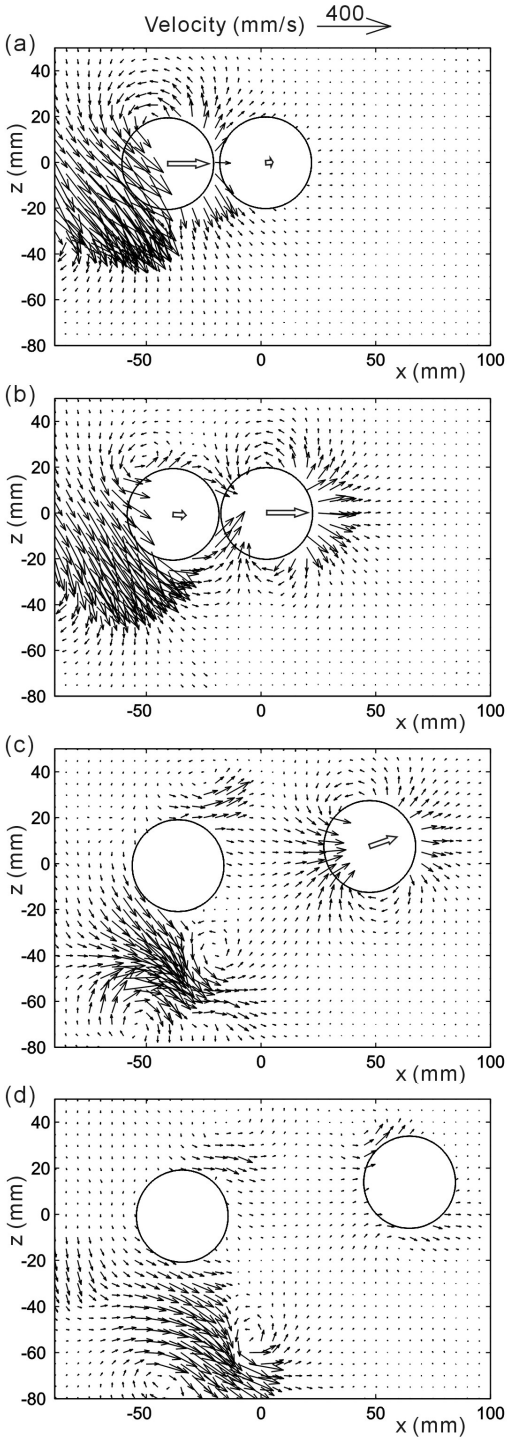

Figure 6

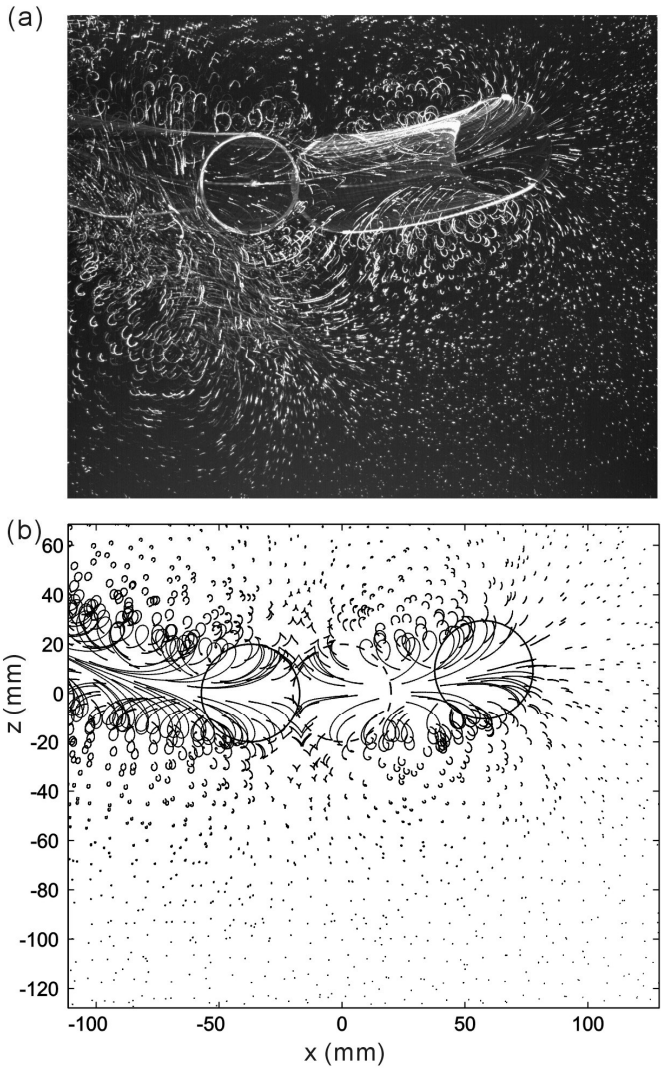

Figure 7